Journal of Energy Storage 121 (2025) 116520

Contents lists available at ScienceDirect

Journal of Energy Storage

journal homepage: www.elsevier.com/locate/est

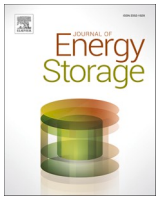

Research papers

Influence of new thermal storage schemes based on modular phase change floors on building heating performance

Tianyu Wang [a], Haichao Wang [a,b,*], Zhiwen Luo [c]

[a] School of Infrastructure Engineering, Dalian University of Technology, Dalian 116024, China
[b] Department of Mathematics and Systems Analysis, Aalto University, School of Science, P.O. BOX 11100, Espoo, Finland
[c] Welsh School of Architecture, Cardiff University, Cardiff, UK

ARTICLE INFO

Keywords:
Phase change floor (PCF)
Local heating
Cascade thermal storage
Energy saving
Numerical simulation

ABSTRACT

The application of convenient modular construction has become a popular building approach. The modularity of phase change floors (PCFs) provides the possibility for flexible heating and energy storage in buildings. This study designs two new thermal storage schemes based on modular PCFs: cascade and partial thermal storage to enhance the PCFs' heating performance. A PCF simulation model is developed and verified by comparing ANSYS simulation results and experimental measurements. Then, heating and cooling processes of PCF heating rooms using different heating methods (full/local) and thermal storage schemes (full/cascade/partial) are comparatively analyzed. The results show that at full heating, the room's thermal comfort is reduced with cascade and partial thermal storage compared to full thermal storage, but the energy efficiency and economic performance are improved with partial thermal storage. Localized overheating of the floor surface occurs with cascade/partial thermal storage. While cascade thermal storage can enhance the melting of phase change materials (PCMs), low-temperature PCMs are prone to incomplete solidification. Partial thermal storage can save up to 2 % of energy over full thermal storage. In addition, with local heating, changes in thermal storage schemes essentially do not affect the room's thermal comfort. Partial thermal storage still offers the best energy efficiency and economic performance. It has a payback period of less than 6.5 years, which is about 2.6 years shorter than full thermal storage. Rooms with different heating methods have different suitable thermal storage schemes.

1. Introduction

With the increasing prominence of environmental issues, energy saving and emission reduction in the building sector have received growing attention. In 2022, building operations accounted for approximately 30 % of global final energy consumption and 26 % of associated carbon emissions [1]. Reducing building emissions is essential to achieving the goal of net-zero emissions. In particular, the spread and application of clean energy technologies significantly reduce carbon emissions during building operations [2]. However, clean energy sources are heavily influenced by geographic factors and often experience an imbalance between heat supply and demand. The emergence of energy storage technology can more effectively address this issue and facilitate the decoupling of heat supply and demand. Currently, common energy storage methods include sensible energy storage, latent energy storage, and chemical energy storage [3]. Phase change floors (PCFs) incorporate phase change materials (PCMs) into the structure of conventional floors. This property of absorbing a substantial amount of latent heat during the PCM phase change is utilized to store energy, which is later released for building heating. Compared to traditional floor heating, PCF heating offers advantages such as energy saving and enhanced thermal comfort. It allows for the flexible storage and utilization of heat generated from clean energy sources and improves indoor thermal comfort [4]. Based on these remarkable properties, researchers have conducted extensive studies on PCFs concerning material, structure, and operational control.

In terms of material, PCM serves as the key thermal storage medium for PCFs, with its thermophysical properties directly influencing the floor's thermal storage capacity and heating effectiveness. The main PCMs commonly utilized in PCFs are paraffin [5] and various composite PCMs [6]. There is an optimal range for both the phase transition temperature and thermal conductivity of the PCM. After comparing different PCM phase transition temperatures, Sun et al. [7] indicated that the optimal phase transition temperature for PCM used in floor thermal storage is between 30 and 31 °C. Furthermore, selecting the optimum phase transition temperature also depends on factors such as

* Corresponding author at: School of Infrastructure Engineering, Dalian University of Technology, Dalian 116024, China.
E-mail address: haichaowang@dlut.edu.cn (H. Wang).

https://doi.org/10.1016/j.est.2025.116520
Received 23 November 2024; Received in revised form 30 March 2025; Accepted 31 March 2025
Available online 7 April 2025

Nomenclature

Abbreviations

PCF	phase change floor
PCMs	phase change materials
MAE	mean absolute error

Symbols

c	specific heat, kJ/kg·°C
h	latent heat, kJ/kg
m	mass, kg
x	simulation value, °C
y	experimental value, °C
α	constant temperature coefficient
β	liquid fraction
ε	emissivity
σ	black-body radiation constant, W/m^2·K^4
λ	thermal conductivity, W/m·°C
ρ	density, kg/m^3
η	energy saving rate
μ	dynamic viscosity, Pa·s
C	electricity price, ¥/kWh
Δt	duration time, h
a	conversion factor between hour and day, h/day
f_t	increase factor of the thermal comfort duration
h_c	convection heat transfer coefficient, W/m^2·K
T_w	unheated surface average temperature, K
Q_{Ed}	average daily electric consumption, kWh

Subscript

p	phase change material
h	heating
c	cooling
s	solid
l	liquid
f	fluid
a	air
MAPE	mean absolute percentage error
RMSE	root mean square deviation
SSP	simple payback period
D	number of heating days, day
H	enthalpy, kJ/kg
N	number
P	pressure, Pa
T	temperature, °C or K
V	velocity vector, m/s
A_{mush}	mushy zone constant
ΔT	difference in temperature, °C
C_d	average daily operating cost, ¥/day
ΔC_{inv}	increased investment costs, ¥
P_h	heating power, kW
Q_p	PCM usage, kg
Q_s	thermal storage capacity, kJ
Q_{sts}	sensible thermal storage capacity, kJ
Q_{lts}	latent thermal storage capacity, kJ
i, j	number of stages
pt	phase transition
ref	refer
tcd	thermal comfort duration
tsr	temperature stable range
inital	heating start moment
end	heating end moment

the material's location within the floor [8], the specific region of application [9], and the supply water temperature for hydronic systems. While an increase in thermal conductivity enhances the indoor temperature rise [10], it can also lead to greater fluctuations in indoor temperatures [11]. Zhou et al. [12] demonstrated that the suitable thermal conductivity for PCM is approximately 0.4 to 0.6 W/(m·°C). Additionally, the greater the latent heat of the PCM, the higher the thermal storage capacity of the floor, which should exceed 120 kJ/kg [13].

In terms of structure, since PCMs typically undergo a solid-liquid phase change in floors, they must be encapsulated, leading to various encapsulation structures such as plates [14] and sheets [15]. Lu et al. [16] designed a double-layer heating coil structure with PCM filling the outer layer of the coil. Some floors employed shape-stable PCMs that did not require encapsulation [17]. The location of the PCM significantly affected the thermal storage and release of the floor. Larwa et al. [18] noted that it was preferable to position the PCM below the heating pipes. To enhance heat transfer, Faraj et al. [19] incorporated staggered spacers and high thermal conductivity copper wires into the PCM, which effectively improved the thermal conductivity of the PCM encapsulation unit. Yu et al. [20] implemented a cascade thermal storage structure with two PCMs featuring different phase transition temperatures arranged vertically, which effectively increased the floor surface temperature. Moreover, such double-layer PCM structures were often utilized for achieving summer cold storage and winter thermal storage in floors [21]. Cesari et al. [22] horizontally staggered two types of PCMs for cold and heat storage respectively in a checkerboard pattern and found that this method provided better energy savings. Unlike the traditional method of filling the PCM in the floor as a whole, Lu et al. [23] designed a casing to fill the PCM only in the external interlayer of the water pipe. This method could solve the problem of slow heating in the traditional filling method, and the melting of PCM could be promoted by reasonably adjusting the position of the water pipe [24].

In terms of operational control, appropriate operational management also impacts the thermal comfort and economic efficiency of PCFs. There are optimal values for both electrical heating power and water supply temperature during the operation of PCFs. Niu et al. [25] pointed out that excessively low electrical heating power hindered the melting and thermal storage of PCMs, while excessively high power could lead to localized overheating. Similarly, problems arose when the water supply temperature was too high. Beak et al. [26] demonstrated that the water supply temperature should exceed the melting point of the PCM, identifying an optimal water supply temperature range of 40 to 41 °C. Additionally, PCFs could effectively shift peak period electricity loads and reduce operating costs by reasonably utilizing peak and valley electricity rates [8]. The control strategy proposed by Barzin et al. [27], based on real-time tariff regulation of room temperature, successfully achieved both a comfortable room temperature and enhanced economic performance. Furthermore, the control strategy developed by Cesari et al. [28], based on outdoor meteorological parameters from weather forecasts, could partially address the issue of indoor overheating. In addition to these three areas of research, other scholars have explored multifaceted studies, including the integrated application of multiple phase change envelopes [29].

As demonstrated by the above analyses, many researchers have conducted studies on PCFs from various perspectives. However, several important issues remain unaddressed in the current study. On the one hand, the energy consumption and operating costs of conventional PCFs remain high. Furthermore, the high price of PCMs contributes to increased investment costs, resulting in longer payback periods for PCFs,

thereby hindering their promotion and application. On the other hand, PCFs are often treated as a single unit in the horizontal direction, which results in this direction being ignored when designing and optimizing PCFs. Previous studies primarily focused on the heat transfer between different materials in the vertical direction of the floor, overlooking the heat transfer processes occurring horizontally. To address these issues, this paper adopts a local heating method with a uniform distribution of the heating zone based on the team's previous research [30]. It also proposes a novel approach to enhance and optimize the energy storage layer of PCFs in the horizontal direction. Unlike previous integrations of multiple PCMs [20,21], this study designs a cascade thermal storage scheme oriented horizontally, combined with the previously described local heating method. Additionally, considering the phase change characteristics of PCMs in the energy storage layer during local heating, the study proposes a partial thermal storage scheme that incorporates PCM at specific locations only. This study modifies the heating and thermal storage methods of PCFs to further improve energy savings and cost-effectiveness in heating applications by reducing heating power, enhancing the melting effect of PCMs, and reducing the quantity of PCMs used. The heat transfer laws in the horizontal direction of the PCF are also investigated. A combination of experimental and simulation methods is employed to simulate the heating and cooling processes of the PCF heating room under full and local heating methods with full, cascade, and partial thermal storage schemes, respectively. The thermal comfort, energy savings, and economics of PCF rooms are analyzed by comparing the average indoor temperature, floor surface temperature, PCM liquid fraction, thermal comfort duration, thermal storage capacity, energy saving rate, and payback period in each room. Clarifying the effects of heating and thermal storage methods on the performance of PCF rooms, as well as designing improved energy consumption and storage solutions, will help reduce floor energy consumption, shorten the payback period, further expand the application of PCFs in buildings, and promote the integration and development of energy storage and heating technologies.

2. Methods

2.1. Geometric models

Based on the research content, the geometrical models established in this paper include the following: fully heated plus fully thermal storage PCF room (FPFR-ful), fully heated plus cascade thermal storage PCF room (FPFR-cas), fully heated plus partial thermal storage PCF room (FPFR-par), locally heated plus fully thermal storage PCF room (LPFR-ful), locally heated plus cascade thermal storage PCF room (LPFR-cas), and locally heated plus partial thermal storage PCF room (LPFR-par). Additionally, a fully heated conventional floor room without PCM thermal storage (FCFR) and a locally heated conventional floor room without PCM thermal storage (LCFR) were also established. The heating and thermal storage methods for the PCF rooms are shown in Table 1. The models are full-size models based on an artificial environment chamber in Dalian, China, with structural dimensions for doors, windows, and other components illustrated in Fig. 1. The PCFs in the room geometry model consist of the electric heating film, the energy storage layer (PCMs), and the floor surface layer (marble), arranged in a bottom-up order. The primary distinction among the six room geometry models lies in their respective heating and thermal storage methods. 'Full heating' refers to the complete activation of the electric heating film during the heating process. The electric heating film power is 0.22 kW/m^2. In contrast, for 'local heating', only a portion of the electric heating film at the position indicated in Fig. 2(a) is activated. The heated area is 71.6 % of the total floor area. The energy storage layer for 'full thermal storage' employs PCM30 as the thermal storage medium. As shown in Fig. 2(b), 'cascade thermal storage' consists of two PCMs, PCM30 and PCM24, which have different phase transition temperatures, with PCM24 placed above the non-heating zone in localized heating scenarios. The floor area ratio between PCM30 and PCM24 is 2.52: 1; 'partial thermal storage' is achieved by avoiding the arrangement of the PCM above the non-heating zone and putting PCM30 in other locations. This study utilizes the PCF module illustrated in Fig. 3 to implement changes in the heating and thermal storage methods. The size of the floor module of the experimental room is 300 × 300 mm, with surface material (marble) thickness of 15 mm and energy storage material (PCMs) thickness of 20 mm.

2.2. Simulation setting

The study was conducted to simulate the heating and cooling processes of PCF heating rooms using ANSYS Fluent software. To simplify the simulation, several common assumptions were adopted: (1) materials such as marble and PCMs are homogeneous and isotropic; (2) the PCM thermophysical parameters are constants, without subcooling and phase separation, ignoring the volume change during its phase transition, and disregarding the natural convection process during the heat transfer of the PCM [31]; (3) the contact thermal resistance between materials is not considered; (4) the temperature of the outer wall surface of the room remains constant; and (5) there is no heat exchange with the external environment at the bottom and perimeter of the floor, which creates an adiabatic condition. The study employed transient simulations, activating the energy equation, melting/solidification model and surface to surface (S2S) radiation model [10]. The enthalpy-porosity method was employed in ANSYS Fluent [32]. There is no need to track the solid-liquid interface, which is represented as a mush zone. The mush zone is considered to be a "pseudo" porous region with a porosity equal to the liquid fraction, which is between 0 and 1. When the material is fully solidified, the porosity is reduced to zero. The control equations for the phase change region and for materials other than PCMs as follows [32–34]:

Energy equation:

$$\rho c \frac{\partial T}{\partial t} = \lambda \, div \, (grad \, T) + S_e \tag{1}$$

Where ρ, c, λ, and T denote density, kg/m^3, specific heat, kJ/kg·°C, thermal conductivity, W/m·°C, and temperature, °C, respectively. S_e is the source term in the energy equation, and in the phase change region $S_e = -\rho \partial h_l / \partial t$, the energy equation can be expressed as:

$$\rho_p \frac{\partial H}{\partial t} = \lambda_p div \, (grad \, T) \tag{2}$$

Where the subscript p refers to the PCM; H consists of the sensible enthalpy h_s and the latent enthalpy h_l.

$$H = h_s + h_l \tag{3}$$

Table 1
Six types of PCF rooms.

Room	FPFR-ful	FPFR-cas	FPFR-par	LPFR-ful	LPFR-cas	LPFR-par
Heating method (Power/kW)	full (3.48)	full (3.48)	full (3.48)	local (2.50)	local (2.50)	local (2.50)
Heat storage method (PCMs)	full (PCM30)	cascade (PCM30 & PCM24)	partial (PCM30 & non-PCM)	full (PCM30)	cascade (PCM30 & PCM24)	partial (PCM30 & non-PCM)

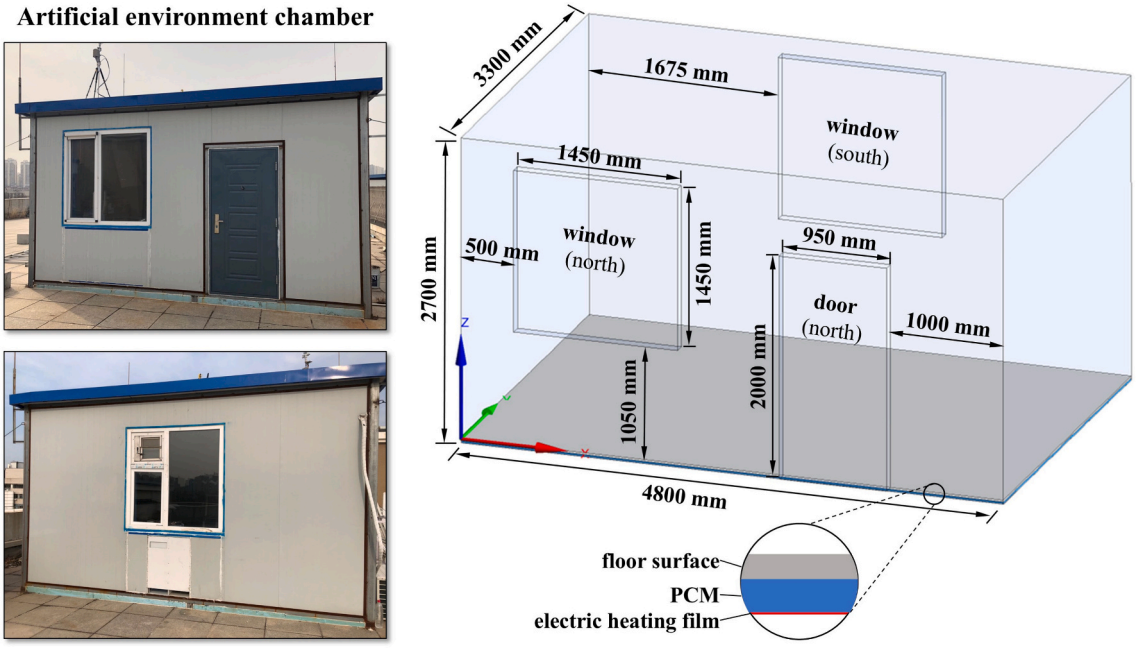

Fig. 1. Artificial environment chamber and geometric model.

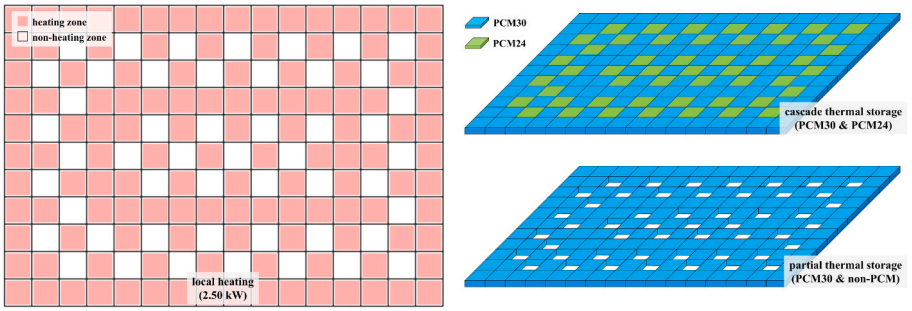

(a) Local heating method (b) Cascade and partial thermal storage methods

Fig. 2. Heating and thermal storage methods.

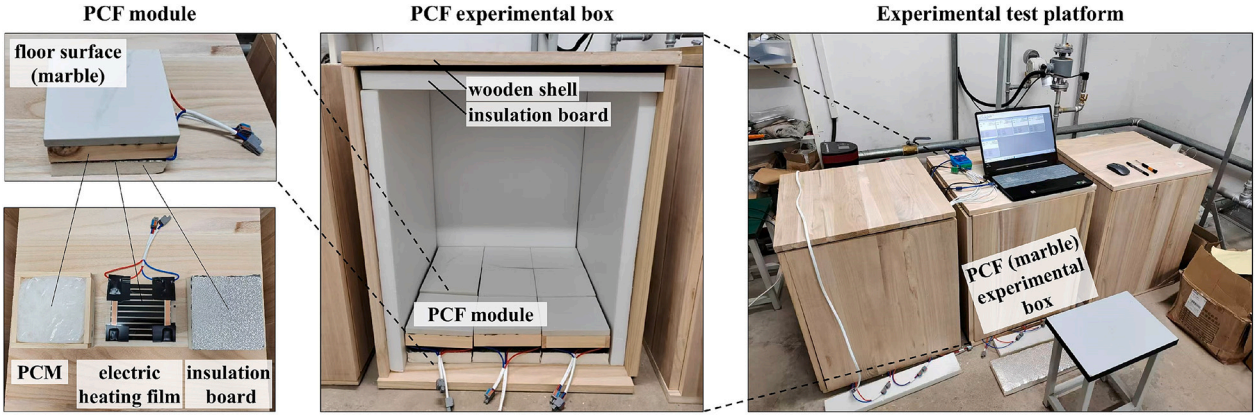

Fig. 3. Experimental test platform.

$$h_s = h_{ref} + \int_{T_{ref}}^{T} c_p dT \quad (4)$$

$$h_l = \beta h \quad (5)$$

$$\beta = \begin{cases} 0, & T < T_s \\ \dfrac{T - T_s}{T_l - T_s}, & T_s < T < T_l \\ 1, & T_l < T \end{cases} \tag{6}$$

Where h_{ref} is the reference enthalpy, kJ/kg; T_{ref} is the reference temperature, °C; β is the liquid fraction; h is the latent heat, kJ/kg; T_s and T_l are the solid and liquid phase temperatures, °C.

Continuity equation:

$$\frac{\partial u}{\partial x} + \frac{\partial v}{\partial y} + \frac{\partial w}{\partial z} = 0 \tag{7}$$

Momentum equation:

$$\rho\left(\frac{\partial V}{\partial t} + (\mathrm{V}\cdot grad)V\right) = \mu\, div\,(grad\, V) - grad\, P + S_m \tag{8}$$

Where V is the velocity vector, m/s; u, v, and w are the velocity components in the x, y, and z directions, m/s; μ is the dynamic viscosity, Pa·s; P is the pressure, Pa. The source term (S_m) in the momentum equation is:

$$S_m = \frac{(1-\beta)^2}{(\beta^3 + q)} A_{mush}\left(\vec{v} - \vec{v}_p\right) \tag{9}$$

Where q is a very small constant preventing division by 0; A_{mush} is the mushy zone constant, taking the default value of 10^5.

The boundary and initial conditions as follows [10,11]:

Perimeter and bottom surfaces of the PCF:

$$\frac{\partial T}{\partial x} = \frac{\partial T}{\partial y} = \frac{\partial T}{\partial z} = 0 \tag{10}$$

The PCM surface inside the PCF is the coupled boundary with continuous temperature and heat flux:

$$T_{(x,y,z,t)}\big|_1 = T_{(x,y,z,t)}\big|_2 \tag{11}$$

$$-\lambda \frac{\partial T}{\partial n}\Big|_1 = h_c\left(T - T_f\right)\big|_2 \tag{12}$$

Upper surface of the PCF:

$$-\lambda \frac{\partial T}{\partial z} = h_c(T - T_a) + \varepsilon\sigma\left(T^4 - T_w^4\right) \tag{13}$$

Exterior wall surfaces of the room:

$$T = -9^{\circ}C \tag{14}$$

initial moment:

$$T_{(x,y,z,t=0)} = 18^{\circ}C \tag{15}$$

Where h_c is the convection heat transfer coefficient, W/m^2·K; ε is the emissivity; σ is the black-body radiation constant, W/m^2·K^4; T_f, T_a and T_w are the fluid, indoor air and unheated surface average temperature, K, respectively.

Two PCMs with different phase transition temperatures were used in the study. The phase transition temperatures of PCM30 and PCM24 were 28–30 °C and 22–24 °C, respectively. Other thermophysical parameters of marble and PCMs are shown in Table 2. Additional material parameters for the walls and other components can be found in the literature [38]. The differences in thermal storage led to variations in the amounts of PCMs used in the room. The amount of PCM30 at full thermal storage was 256.61 kg. The amounts of PCM30 and PCM24 at cascade thermal storage were 183.71 kg and 79.2 kg, respectively. The 183.71 kg of PCM30 was allocated for partial thermal storage. The initial room temperature was set to 18°C. The outer wall surface temperature was set to −9°C [39]. The study simulated one complete heating and cooling cycle for each room. During the heating process, the average indoor temperature increased from 18to 24 °C. Then, the heating was stopped, and the cooling process began. It was over when the average indoor temperature returned to 18 °C.

Table 2
Thermophysical properties of materials.

Materials	T_{pt} (°C)	h (kJ/kg)	ρ (kg/m^3)	c (kJ/kg·°C)	λ (W/m·°C)
PCM30 [35]	28–30	150	810	2.14	0.21
PCM24 [36]	22–24	150	880	2	0.2
marble [37]	–	–	2800	1	3.5

2.3. Model validation

To verify the accuracy of the simulation results, this study conducted a comparative analysis of the experimental and simulated data. A small-size experimental test platform was constructed, as shown in Fig. 3. Heating and cooling tests were performed for both full heating (where 9PCF modules were heated) and local cross-heating (where 5 PCF modules were heated) by adjusting the number of activated electric heating films in the PCF experimental box. The air temperature was monitored at a vertical distance of 200 mm from the floor surface. The accuracy of the temperature sensor (Probe 485 type) [40] used was ±0.3 °C, with an applicable range of −40 to 80 °C. Both the full and local heating experiments were conducted six times, and the average temperatures were recorded as experimental data. Meanwhile, the same PCF box simulation platform was constructed, and the temperature variations during the heating and cooling processes at the same location under identical heating conditions were recorded as simulation data.

From Fig. 4, it is evident that the temperature variation trend over time is consistent between the experimental data and the simulated data during the heating and cooling processes. Although a slight discrepancy exists between the two data sets due to factors such as inconsistencies in the initial temperature of the box and variable outside temperatures during the actual test, the maximum temperature deviation does not exceed 0.6 °C, and the maximum absolute error is only 2.25 %. Meanwhile, the root mean square error (RMSE), mean absolute error (MAE), and mean absolute percentage error (MAPE) calculated from Eqs. (16)~(18) [41] are 0.27 °C, 0.23 °C, and 0.97 %, respectively, during full heating. For local heating, these values are 0.13 °C, 0.1 °C, and 0.45 %, respectively. This demonstrates the accuracy and feasibility of analyzing the heating and cooling processes of PCFs using simulation methods. Furthermore, to ensure the accuracy of the simulation results while

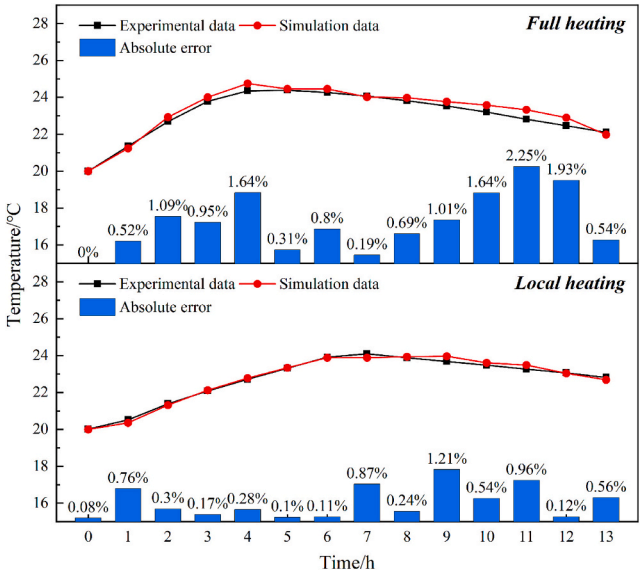

Fig. 4. Experimental validation.

saving computational power and time, a mesh number of 1.6×10^6 and a time step of 10 s were selected for the study. This decision is based on the observation that the effect of changes in mesh number on temperature clearly diminishes when the mesh number exceeds 1.6×10^6, as illustrated in Fig. 5. Additionally, as the time step increases from 1 s to 20 s, the temperature variations remain minimal. Notably, when the time step is less than 10 s, the simulation results are essentially unaffected by changes in the time step.

$$RMSE = \sqrt{\sum_{i=1}^{N} \frac{(x_i - y_i)^2}{N}} \tag{16}$$

$$MAE = \sum_{i=1}^{N} \frac{|x_i - y_i|}{N} \tag{17}$$

$$MAPE = \frac{1}{N} \sum_{i=1}^{N} \left| \frac{x_i - y_i}{y_i} \right| \times 100\% \tag{18}$$

Where N is the number; x_i and y_i are the simulated and experimental values at moment i, respectively, °C.

2.4. Evaluation indicators

The study comparatively analyzes the variation trends of the average indoor temperature, floor surface temperature, and PCM liquid fraction in each room throughout a heating and cooling cycle. Additionally, the indoor thermal comfort, energy savings, and economic performance of PCF heating rooms are evaluated using the following indicators.

(1) Heating and cooling time (Δt_h and Δt_c)

Heating time is defined as the duration required to raise the average indoor temperature from 18 to 24 °C. This period corresponds to the time during which the electric heating film remains activated within the heating and cooling cycle.

Cooling time refers to the duration taken after the electric heating film is turned off until the average room temperature is reduced back to 18 °C.

(2) Thermal comfort duration time (Δt_{tcd}) and its increase factor (f_t) [42]

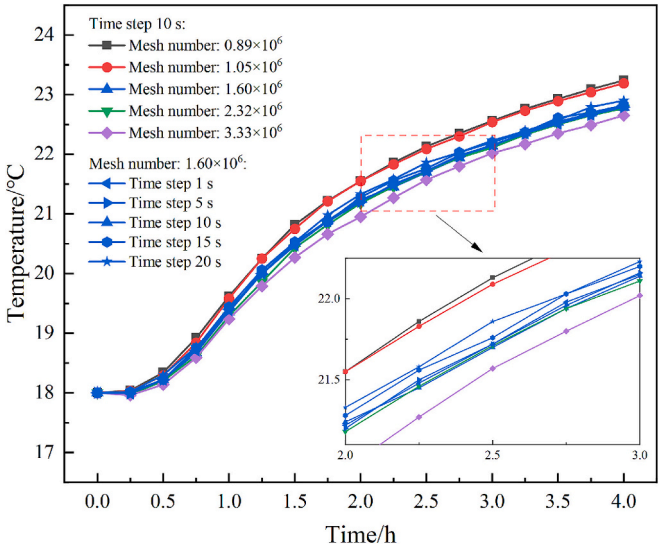

Fig. 5. Independence test.

Thermal comfort duration represents the time during which the average indoor temperature can be maintained within the thermal comfort range (18–24 °C [43]) throughout a heating and cooling cycle. It consists of the thermal comfort duration during the heating process ($\Delta t_{tcd,h}$) and the cooling process ($\Delta t_{tcd,c}$). Since the average indoor temperature may be lower than 18 °C at the beginning of the heating process, $\Delta t_{tcd,h}$ does not equal Δt_h. Furthermore, the average indoor temperature may exceed 24 °C after the electric heating film is turned off, resulting in $\Delta t_{tcd,c}$ being less than Δt_c.

The increase factor (f_t) is the ratio of the thermal comfort duration in the PCF room to that in the reference room, where heating relies solely on the stored heat of the floor after the electric heating film has been switched off (cooling process).

$$f_t = \Delta t_{tcd,c,ref} / \Delta t_{tcd,c} \tag{19}$$

Where $\Delta t_{tcd,c,ref}$ is the thermal comfort duration of the reference room during cooling, h.

(3) Relative stable temperature (T_{tsr}) and stable duration time (Δt_{tsr})

In a PCF heating room, there exists a time range where the average indoor temperature varies minimally. This range reflects indoor thermal comfort to some extent. Therefore, this study introduces two indicators to evaluate it in terms of both temperature and duration. The relative stable temperature (T_{tsr}) and stable duration time (Δt_{tsr}) represent the relative average temperature at which the stability condition (Eqs. (21) and (22)) is met and the duration for which it can be sustained. This paper assumes that the temperature remains stable if it does not change by more than 0.01 °C/min.

$$T_{tsr} = \frac{1}{N} \sum_{i=1}^{N} T_{tsr,i} \tag{20}$$

$$\left| T_{tsr,i+1} - T_{tsr,i} \right| \le \alpha (T_{end} - T_{inital}) \tag{21}$$

$$T_{inital} < T_{ctr,i} < T_{end} \tag{22}$$

Where $T_{tsr,i}$ and $T_{tsr,i+1}$ are the temperatures at the moments i and $i+1$ that satisfy the temperature stabilization condition, °C, respectively; α is the thermostatic coefficient, set at 5 %; T_{inital} and T_{end} are the temperatures at the beginning (18 °C) and end (24 °C) of the heating process, °C, respectively.

(4) Thermal storage capacity (Q_s) [44]

The thermal storage capacity of the PCF comprises both the sensible (Q_{sts}) and latent (Q_{lts}) thermal storage capacities of the PCM.

$$Q_s = Q_{sts} + Q_{lts} = c_p m_p \Delta T_p + \beta m_p h \tag{23}$$

Where m_p is the mass of PCM, kg/m^3; ΔT_p is the temperature change of PCM during the heating process, °C.

(5) Average daily electric consumption (Q_{Ed}) and Energy saving rate (η) [9]

Based on the average daily electricity cost [33], the average daily electric consumption (Q_{Ed}) of a room with PCF can be expressed as:

$$Q_{Ed} = \frac{a P_h \Delta t_h}{\Delta t_h + \Delta t_c} \tag{24}$$

Where P_h is the electric heating film power, kW; a is the conversion factor between day and hour, 24 h/day.

The energy saving rate (η) is the ratio of the energy saved in the PCF room compared to the reference room relative to the energy consumption of the reference room.

$$\eta = \frac{Q_{Ed,\mathrm{ref}} - Q_{Ed}}{Q_{Ed,\mathrm{ref}}} \tag{25}$$

Where $Q_{Ed,\mathrm{ref}}$ is the average daily electric consumption of the reference room, kWh/day.

(6) Average daily operating cost (C_d) [33] and simple payback period (SSP) [19]

The average daily operating cost (C_d) considers the differences in electricity prices during peak and valley periods. According to the peak and valley electric power tariff policy [45,46], the peak, level and valley periods span 8 h each day, with tariffs of 1.03 ¥/kWh, 0.71 ¥/kWh and 0.39 ¥/kWh, respectively.

$$C_d = \frac{aP_{\mathrm{h}}\sum_{j=1}^{3} C_j \Delta t_{\mathrm{h},j}}{\Delta t_{\mathrm{h}} + \Delta t_{\mathrm{c}}} \tag{26}$$

where C_j and $\Delta t_{\mathrm{h},j}$ represent the electricity price, ¥/kWh, and the heating time, h, for period j, respectively; $j = 1,2,3$ refer to the peak, level, and valley periods, respectively.

The simple payback period (SSP) indicates the time required to recover the additional cost of the PCF room compared to the reference room.

$$SSP = \frac{\Delta C_{inv}}{D\left(C_{d,\mathrm{ref}} - C_d\right)} \tag{27}$$

$$\Delta C_{inv} = Q_p C_p \tag{28}$$

where ΔC_{inv} is the investment cost of the PCF room over the reference room, ¥, primarily reflecting the increased PCM cost. Q_p is the amount of PCM used, kg; C_p is the price of PCM, ¥/kg, assuming the price for both PCM30 and PCM24 is 50 ¥/kg [35]; D is the number of heating days, day, 125 days [39] in this study; and $C_{d,\mathrm{ref}}$ is the average daily operating cost of the reference room, ¥/day.

3. Results and discussion

3.1. Thermal comfort analysis

3.1.1. Average indoor temperature

During a heating and cooling cycle, the average indoor temperature first rises and then falls over time, as shown in Fig. 6. When the full heating method is employed, Fig. 6(a) demonstrates that different thermal storage methods significantly affect indoor temperature variations. Compared to FPFR-ful, FPFR-cas, which uses cascade thermal storage, notably reduces the indoor temperature during both heating and cooling. At the same time, the average indoor temperature is reduced by up to about 2.7 °C. Although the heating time is roughly the same for both methods (around 6 h), FPFR-ful has a cooling time approximately 2.81 h longer than FPFR-cas. This indicates that, under identical operating conditions as the electric heating film, the thermal storage method of FPFR-ful results in higher room temperatures and a longer duration of room heating. Additionally, compared to FPFR-ful and FPFR-cas, the heating and cooling times for FPFR-par are relatively shorter, at 2.83 h and 9.09 h, respectively. The operating time of its electric heating film is about 1.65 h longer than that of FCFR, which does not include PCM. The cooling time for FPFR-par is about 4.94 h longer than that of FCFR due to its thermal storage ability. This suggests that introducing PCM as a thermal storage medium in the full heating method generally prolongs both heating and cooling times. Moreover, the cooling times across methods—no thermal storage, partial thermal storage, cascade thermal storage, and full thermal storage—progressively increase.

Under the local heating method, the average indoor temperatures in rooms with full, cascade, and partial thermal storage show minimal differences, as depicted in Fig. 6(b). Additionally, the heating and cooling times show less variation between these methods. Specifically, the difference between the average indoor temperatures of LPFR-ful and LPFR-cas is less than 0.2 °C. The LPFR-par's indoor temperature is slightly lower than the other two, but the maximum temperature difference is only around 0.8 °C. Furthermore, all three methods have similar heating times (around 7.6 h) and cooling times (around 14.8 h), with differences not exceeding 0.5 h. Compared to LCFR, they increase the heating time by about 6 h and the cooling time by about 11 h. This indicates that, under the local heating method, the thermal storage method has a less significant impact on temperature variation, as well as on the heating and cooling times. The introduction of PCM likewise increases the heating and cooling times.

However, as shown in Fig. 6, different heating methods can substantially influence the heating and cooling processes of a room when the thermal storage methods remain the same. With full thermal storage, FPFR-ful has a shorter heating time and a longer cooling time compared to LPFR-ful. A similar trend is observed with cascade thermal storage, albeit to a lesser extent. Compared to LPFR-cas, the heating time of FPFR-cas is reduced by approximately 1.88 h, while the cooling time is

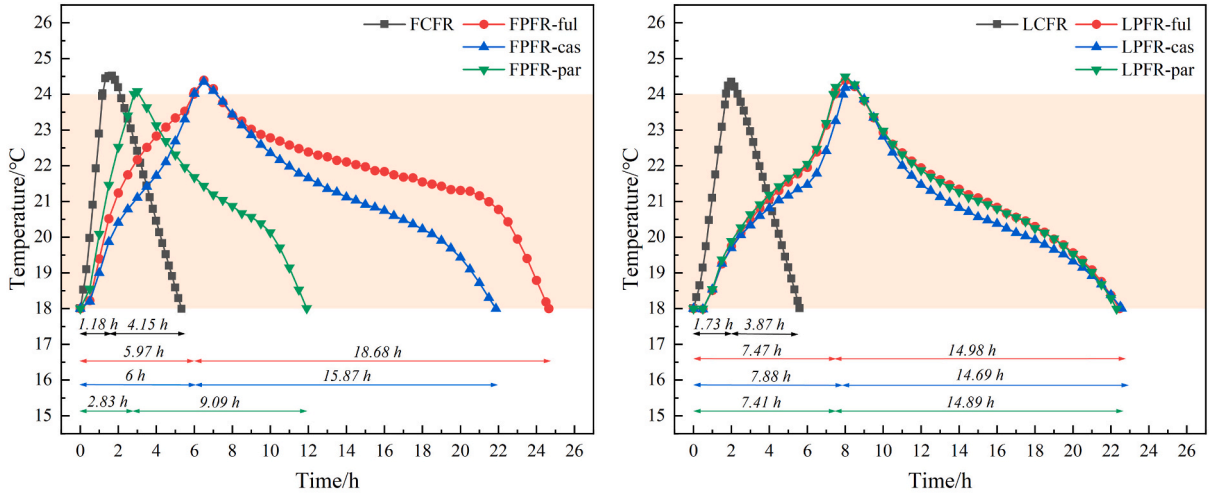

(a) Full heating (b) Local heating

Fig. 6. Variation of average indoor temperature over time.

extended by 1.18 h. Additionally, with partial thermal storage, the heating time remains shorter with full heating, and the cooling time is considerably lower than that of local heating. This is mainly because the short heating time of FPFR-par does not allow the PCM to fully melt and store heat, and there is not enough heat to be released during cooling, so its cooling time is shorter. LPFR-par has a longer heating time, which allows the PCM to melt more fully, and more heat is released during cooling, so its cooling time is longer. LPFR-par has about 5.8 h more cooling time than FPFR-par.

3.1.2. Thermal comfort duration and room temperature stable range

Fig. 7 illustrates the thermal comfort duration and its increase factor for a room with PCF. As depicted in the figure, the cooling process allows the room to maintain a thermally comfortable temperature for a significantly longer period, approximately twice as long as during the heating process. Throughout both heating and cooling processes, FPFR-par exhibits the shortest thermal comfort duration, with values of $\Delta t_{tcd,h}$ and $\Delta t_{tcd,c}$ being only 2.83 h and 8.83 h, respectively. Although LPFR-cas has the highest $\Delta t_{tcd,h}$ value, its $\Delta t_{tcd,c}$ does not exceed 13.8 h. During the cooling process, FPFR-ful achieves the longest duration of thermal comfort at 17.44 h and also has the highest total thermal comfort duration, exceeding 23 h. The total thermal comfort duration in all other rooms (except FPFR-ful and FPFR-par) is around 20 h. Moreover, although the cooling time of FCFR is longer than that of LCFR, the average indoor temperature of FCFR is above 24 °C for a longer period, which leads to essentially the same $\Delta t_{tcd,c}$ values for both. Using FCFR as the reference room, the thermal comfort duration increase factor exceeds 2.5 for each room with PCF. This indicates that PCF rooms can sustain temperatures between 18 °C and 24 °C for a longer duration after the electric heating film is turned off. All rooms, except FPFR-par, have f_t values above 4. The f_t value for FPFR-ful is even higher at 5.40.

Considering the existence of room temperature stable ranges in PCF heating rooms, the study presents Fig. 8, which shows the relative stable temperatures and durations for each room. As indicated in the figure, the relative stable temperatures are predominantly within the range of 20.5 to 21.5 °C, with their $T_{tsr,c}$ values slightly lower than the $T_{tsr,h}$ values. Due to the increased use of PCM30 in FPFR-ful and its higher phase transition temperature compared to PCM24, both $T_{tsr,h}$ and $T_{tsr,c}$ values for FPFR-ful are relatively high, reaching 23.19 °C and 22.01 °C, respectively. Compared to LPFR-ful, FPFR-ful can increase the T_{tsr} value by more than 1 °C. Additionally, the value of Δt_{tsr} is greater during cooling than heating in each room. This is attributed to the thermal inertia of the PCM, with room heating during the cooling process relying mainly on the release of latent heat from the PCM. Their Δt_{tsr} values do

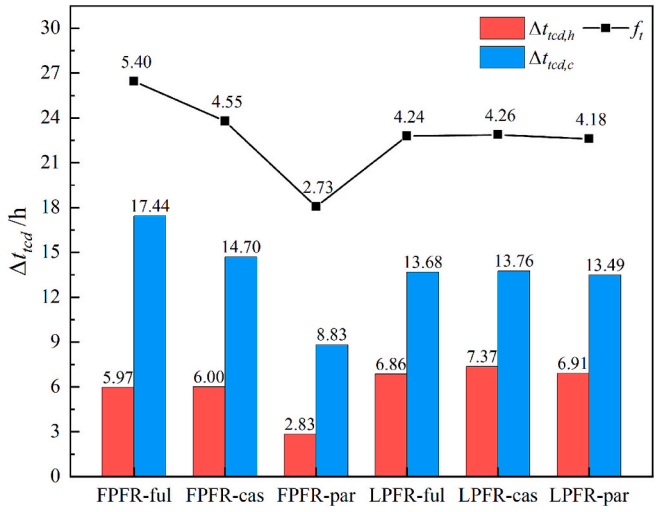

Fig. 7. Thermal comfort duration and its increase factor.

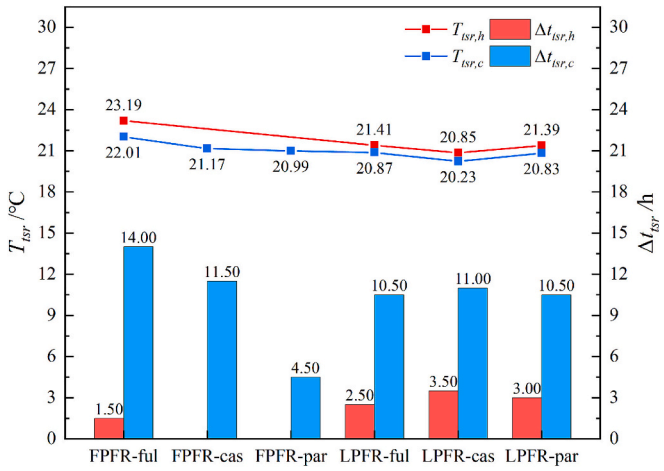

Fig. 8. Relative stable temperature and duration.

not exceed 3.5 h for heating and do not fall below 10.5 h for cooling. FPFR-ful can maintain a steady temperature for the longest duration. Moreover, the room temperature stable ranges for FPFR-cas and FPFR-par exist only during cooling. When heating, the room temperature stable ranges do not exist for both due to their higher heating power, lower PCM phase transition temperatures, and less PCM usage, which leads to a faster increase in room temperature.

3.1.3. Floor surface temperature

Fig. 9 illustrates the temperature distribution on the floor surface at the end of the heating process. As depicted in the figure, the distribution of floor surface temperatures under different thermal storage methods exhibits significant variations when fully heated. Specifically, the floor surface temperature of FPFT-ful is roughly maintained at 30 to 32 °C, with a minimal temperature difference across its surface. In contrast, the temperature distributions in FPFR-cas and FPFR-par clearly indicate a trend where the floor surface temperature above the PCM24 position (and areas without PCM) is higher than in other regions. This is attributed to the lower melting point of PCM24 used in certain areas of FPFR-cas, allowing it to initiate the phase change more rapidly and melt completely. By the end of the heating process, PCM24 has been undergoing sensible thermal storage for some time, leading to an accelerated temperature rise. The temperature of PCM24 significantly exceeds that of PCM30, which is still undergoing phase change at the phase transition temperature, resulting in a higher floor surface temperature above it. Furthermore, some regions in FPFR-par are not filled with PCM, lacking latent thermal storage ability. The electric heating film transfers heat directly through the air to the floor surface, resulting in a higher floor surface temperature in this region, with a maximum value exceeding 38 °C. Compared to FPFR-cas, FPFR-par displays a higher maximum floor surface temperature and a lower minimum temperature, with a maximum temperature difference of about 13 °C.

For the local heating method, the floor surface temperature distribution across all three thermal storage methods is higher in the heating zone and lower in the non-heating zone. Moreover, the temperature distributions in LPFR-ful and LPFR-par are remarkably similar, with their highest and lowest temperatures recorded at 37.5 °C and 23.5 °C, respectively. In contrast, the temperature difference on the floor surface of LPFR-cas is relatively larger, reaching a maximum temperature difference of 16 °C. Additionally, different heating methods can lead to varied floor surface temperature distributions when employing the same thermal storage method. It is evident that the temperature difference on the floor surface is generally greater with local heating. When a full thermal storage method is employed, the maximum temperature difference on the floor surface can reach up to 14 °C for LPFR-ful, whereas for FPFR-ful, it does not exceed 6 °C. Meanwhile, the temperature

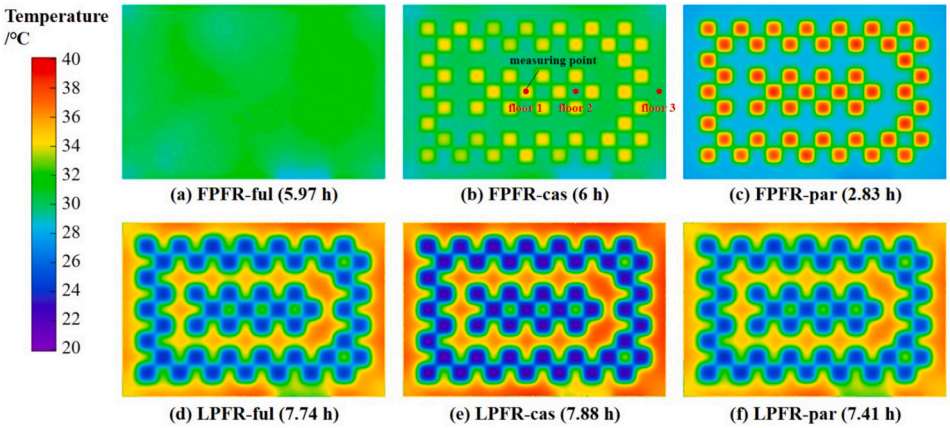

Fig. 9. Temperature distribution on the floor surface at the end of the heating process (heating time).

difference for LPFR-cas is approximately 6 °C higher compared to FPFR-cas when utilizing the cascade thermal storage method. However, the temperature difference between LPFR-par and FPFR-par, both utilizing partial thermal storage, is essentially the same. Thus, regardless of the thermal storage method employed, the issue of localized overheating on the floor surface with local heating becomes more pronounced by the end of the heating process.

Based on the temperature distribution of the floor surface presented in Fig. 9, three temperature measurement points—floor1 ($x = 2250$ mm, $y = 1650$ mm), floor2 ($x = 3150$ mm, $y = 1650$ mm), and floor3 ($x = 4650$ mm, $y = 1650$ mm)—located on the floor surface, as shown in Fig. 9(b), were selected for the study. A dimensionless time t^* [47], defined as the ratio of any moment to the total heating and cooling cycle time, was used to facilitate the comparative analysis of the temperature variation over time on the floor surface in each room (Fig. 10). To meet thermal comfort requirements, the floor surface temperature should typically remain above 25 °C and not exceed 29 °C for individuals staying for long periods or 32 °C for short periods [48]. As illustrated in Fig. 10(a), during full heating, the floor surface temperature of FPFR-ful remains consistent throughout the heating and cooling processes, maintaining thermal comfort for an extended period. While in FPFR-cas, the floor1 point, located above PCM24, is affected by the low phase transition temperature, which is significantly lower and cannot reach 25 °C for a long time. In addition, since there is no latent thermal storage in FPFR-par, the temperature at the floor1 point rises rapidly during the heating process, exceeding 32 °C. Its temperature decreases sharply during the cooling process. In contrast, the trend of the floor surface temperature over time remains largely consistent across the three thermal storage methods in the local heating method, as shown in Fig. 10(b). Since floor1 is positioned above the non-heating zone, its temperature remains low throughout both the heating and cooling processes. Meanwhile, the temperatures at the floor2 and floor3 points are largely maintained between 25 °C and 30 °C. Additionally, floor2, which is located in an unheated area on the perimeter, is generally cooler than floor3. Although the variations in floor surface temperatures differ across the various thermal storage methods in Fig. 10(a), they converge in Fig. 10(b). This indicates that the heating method has a more significant impact on the floor surface temperature than the thermal storage method.

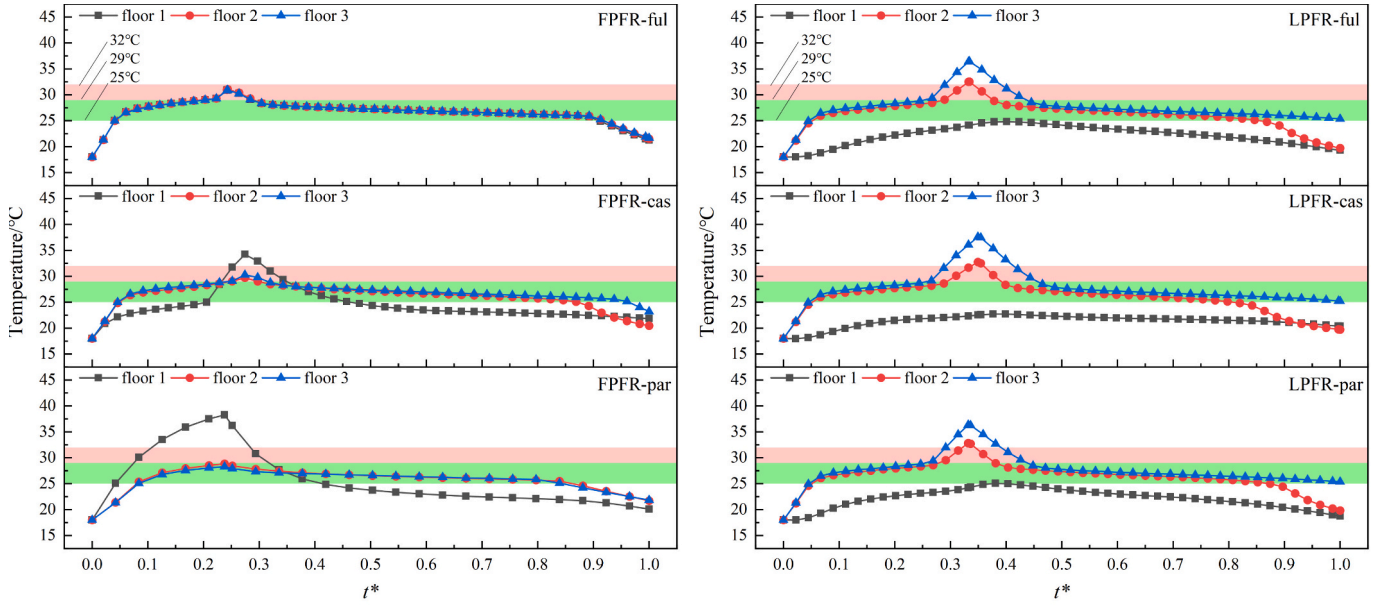

Fig. 10. Variation of floor surface temperature over time.

3.2. Energy saving and economic analysis

3.2.1. PCM liquid fraction and thermal storage capacity

Fig. 11 illustrates the variation in the average liquid fraction over time for different PCMs across various rooms. The figure clearly shows that, under full heating conditions, both PCM30 and PCM24 can be completely melted in all thermal storage methods except FPFR-par, where their liquid fraction reaches 1. In FPFR-par, there are regions where PCM is not incorporated, causing the electric heating film in these areas to transfer heat directly through the air to the floor surface. This heat subsequently warms the room, resulting in a rapid increase in the average indoor temperature (Fig. 6(a)). Consequently, this configuration leads to a shorter heating time for FPFR-par. However, this brief heating period prevents the complete melting of PCM30 in FPFR-par, resulting in its liquid fraction not reaching 0.5, as shown in Fig. 11(a). Additionally, while the PCM in FPFR-ful and FPFR-cas melts effectively, PCM24 (in FPFR-cas) exhibits poor solidification during the cooling process. This is primarily due to PCM24's low phase transition temperature, which makes it challenging to lower its temperature to the solidification point during cooling. By the end of the cooling process, the liquid fraction of PCM24 remains at 0.8. In contrast, PCM30, having a higher phase transition temperature, begins to solidify more quickly. Consequently, its liquid fraction can be reduced to 0 in both FPFR-ful and FPFR-cas, indicating complete solidification.

Unlike full heating, the phase change of the PCM inside the LPFR-par is more effective than that in the other two thermal storage methods during local heating, as shown in Fig. 11(b). PCM30 (LPFR-par) is fully utilized, melting and solidifying completely by the end of the heating and cooling processes. In contrast, the liquid fraction of PCM30 within LPFR-ful is only 0.7 at the end of heating, indicating that part of the PCM is not completely melted and that the added PCM30 is insufficiently utilized. In LPFR-cas, the two added PCMs also exhibit significant differences in the degree of phase change during heating and cooling. Since PCM30 is located above the heating zone, it begins to melt before PCM24, despite having a higher phase transition temperature. Furthermore, because the temperature of PCM30 is higher than that of PCM24, it transfers some of its heat to PCM24, causing PCM24 to continue melting for some time even after heating has ended. Moreover, due to the influence of low-temperature PCM24, even though the position and amount of PCM30 in LPFR-cas and LPFR-par are the same, the melting effect of PCM30 in LPFR-cas is slightly inferior to that in LPFR-par. Additionally, an analysis of the different heating methods shows that when full thermal storage is employed, since some electric heating films are not turned on during local heating and the thermal conductivity of PCM is low, the PCM above the non-heating zone is difficult to sufficiently heat to fully melt under the same heating time. This results in the melting effect of PCM30 during local heating being significantly inferior to that during full heating. In the case of cascade thermal storage, regardless of the heating method used, the melting of PCM30 in the floor is more effective, while PCM24 suffers from incomplete solidification. In the partial thermal storage method, the phase change situation of PCM30 during local heating is considerably better than during full heating.

Fig. 12 summarizes the sensible thermal storage capacity (Q_{sts}), latent thermal storage capacity (Q_{lts}), and total thermal storage capacity (Q_{tts}) for the PCF room. As shown in the figure, PCF thermal storage is predominantly influenced by latent thermal storage, with the proportion of latent thermal storage in each room exceeding 75 % of the total thermal storage. Changes in thermal storage capacity primarily reflect increases or decreases in latent thermal storage, while variations in sensible thermal storage capacity do not exceed 5 MJ. In the full heating method, the PCMs in both FPFR-ful and FPFR-cas can be completely melted, allowing them to store a relatively large amount of heat—approximately 48 MJ. In contrast, FPFR-par, where the PCM is

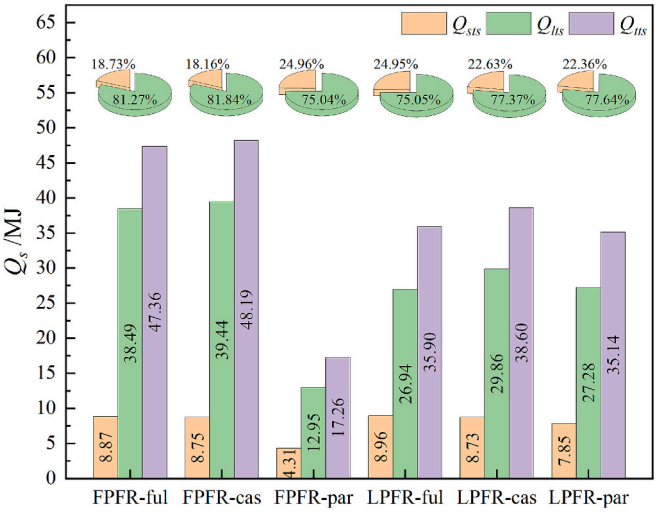

Fig. 12. Thermal storage capacity of PCF rooms.

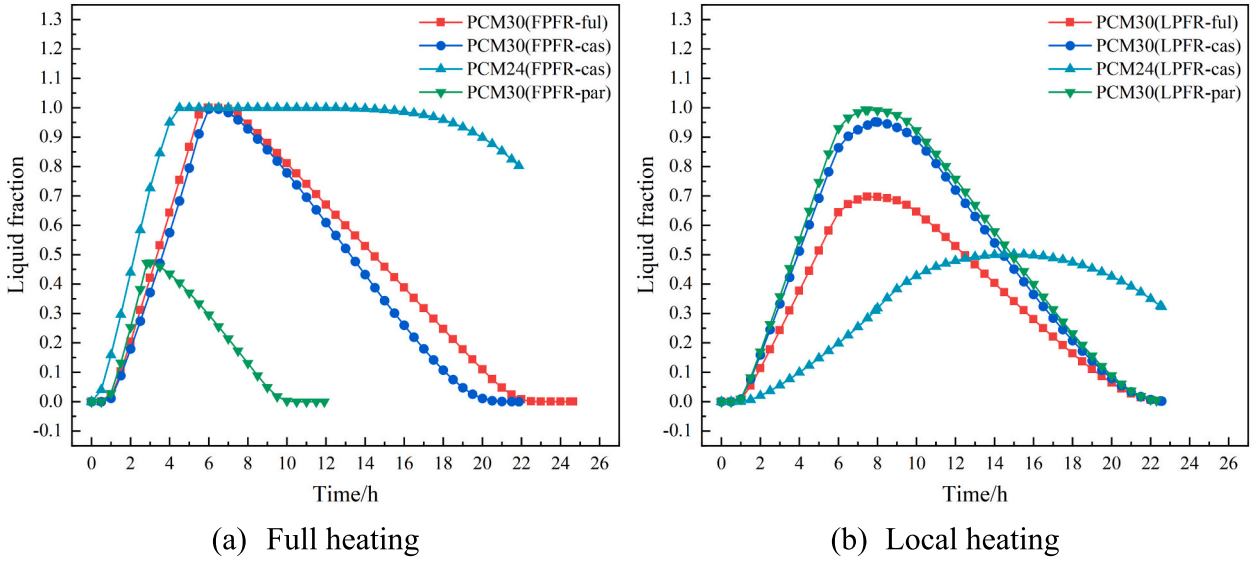

Fig. 11. Variation of PCM liquid fraction over time.

not fully melted, stores significantly less heat than the other two methods. This results in insufficient thermal energy to heat the room during the cooling process, leading to an extremely short cooling time, as previously described. For local heating, among the three thermal storage methods, the cascade thermal storage method exhibits the highest stored heat. Compared to LPFR-ful and LPFR-par, the thermal storage capacity of LPFR-cas increased by approximately 7.5 % and 9.8 %, respectively. This is primarily because PCM24, located above the non-heating zone in LPFR-cas, contributes to a certain amount of latent thermal storage. LPFR-cas can store about 3 MJ more latent thermal capacity. The thermal energy storage potential of LPFR-ful and LPFR-par is essentially equivalent, with a difference of no more than 0.8 MJ. Additionally, the amount of thermal energy stored when fully heated is generally higher than when locally heated for rooms with full and cascade thermal storage. Conversely, when employing the partial thermal storage method, the heat stored in a room with full heating is significantly lower than that achieved with local heating, with LPFR-par exhibiting approximately double the thermal storage capacity compared to FPFR-par.

3.2.2. Average daily electric consumption and energy saving rate

Fig. 13 shows the average daily electric consumption and energy saving rate for each room. As shown in the figure, the Q_{Ed} values for all rooms, except FPFR-cas, are essentially equal, at approximately 20 kWh/day. This is primarily because the Q_{Ed} value of the room depends on the amount of heating power and the durations of heating and cooling times. Under full heating conditions, although the cooling time for FPFR-par is significantly shorter than that for FPFR-ful, its heating time is also relatively short; thus, the operating time of the electric heating film is reduced. Consequently, the Q_{Ed} values for both rooms are essentially equal, with the Q_{Ed} value for FPFR-ful being slightly higher than that for FPFR-par by about 0.4 kWh/day. Additionally, since the heating and cooling times of the three thermal storage methods are similar for local heating, the differences in their Q_{Ed} values are minimal, not exceeding 1 kWh/day. However, FPFR-cas exhibits a notably shorter cooling time compared to FPFR-ful, despite both having the same heating time, resulting in a higher Q_{Ed} value of 22.95 kWh/day. Furthermore, while LPFR-ful and LPFR-par require longer heating times and shorter cooling times under local heating compared to full heating, their Q_{Ed} values do not differ significantly because the heating power of both is only 72 % of that during full heating. Conversely, for the cascade thermal storage method, transitioning from full heating to local heating leads to a relatively large variation in the Q_{Ed} value, decreasing by about 8.9 %. Using FPFR-ful as a reference room, the energy saving rates for FPFR-par, LPFR-ful, and LPFR-par are higher than that of FPFR-ful. The energy saving rates of the three rooms are 2 %, 1.6 %, and 1.8 %, respectively. This indicates that they can achieve further energy savings beyond those of traditional PCFs with full heating and full thermal storage.

3.2.3. Average daily operating cost and simple payback period

From the analyses above, it is evident that the heating time for all rooms utilizing PCF heating is less than 8 h. Consequently, the study set the heating process of the PCF rooms to operate entirely during the valley electricity period, while the reference room (FCFR) operates during the peak electricity period. Compared to the FCFR, the additional investment for each PCF room primarily involves the increased cost of PCMs. The increased PCM costs are 12.83×10^3 ¥, 13.15×10^3 ¥, and 9.19×10^3 ¥ for full, cascade, and partial thermal storage, respectively. This results in the average daily operating costs and simple payback periods for each room, as shown in Fig. 14. Since the electric heating film in each PCF room operates at an electricity price of 0.39 ¥/kWh, the variations of the average daily operating costs in the rooms with different heating and thermal storage methods mirror the variations of the average daily electric consumption. Among these, FPFR-cas has the highest C_d value, exceeding 9 ¥/day, while FPFR-par has the lowest C_d value, which is 1.21 ¥/day lower than that of FPFR-cas. The C_d values for the other rooms are approximately 8 ¥/day. FCFR has a C_d value of about 36.34 ¥/day. Additionally, the differing investment costs lead to variations in the simple payback periods across the rooms. Regardless of whether full or local heating is applied, rooms utilizing cascade thermal storage incur the highest incremental costs and average daily operating costs, resulting in the longest payback period of over 9.5 years. For the other two types of thermal storage, although the C_d values for the partial and full thermal storage rooms are generally equal, partial thermal storage requires less PCM and incurs a lower incremental cost, resulting in a shorter payback period. Rooms with partial thermal storage can generally achieve cost recovery within 6.5 years.

4. Conclusion

In this study, several PCF heated rooms with different heating methods and thermal storage schemes were simulated and analyzed. By comparing the heating and cooling processes of each room utilizing full, cascade, and partial thermal storage for both full and local heating methods, the study investigated the variation of average indoor temperature, floor surface temperature, and PCM liquid fraction over time in each room. Additionally, the thermal comfort, energy savings, and economic viability of the rooms were evaluated using indicators such as thermal comfort duration, energy saving rate, simple payback period, and so on. The conclusions drawn are as follows:

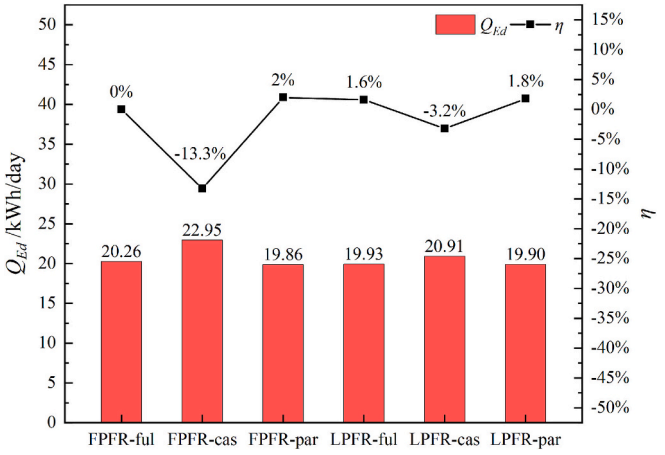

Fig. 13. Average daily electric consumption and energy saving rate.

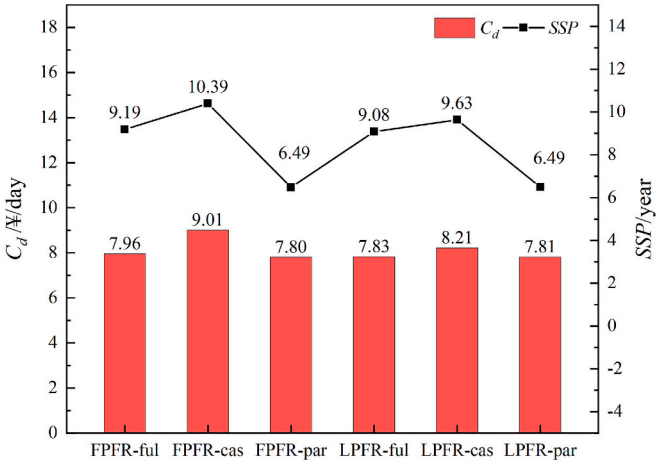

Fig. 14. Average daily operating cost and simple payback period.

(1) When a full heating method is employed, different thermal storage methods significantly affect the thermal comfort, energy saving, and economic viability of PCF heating rooms. Full thermal storage (FPFR-ful), cascade thermal storage (FPFR-cas), and partial thermal storage (FPFR-par) rooms exhibit progressively decreasing levels of indoor thermal comfort. FPFR-ful has the longest cooling time, with f_t value up to 5.40, and the higher indoor temperature, with T_{tsr} value over 22 °C. Localized overheating of the floor surface is observed in both FPFR-cas and FPFR-par, with the issue being more pronounced in FPFR-par. Furthermore, when compared to FPFR-ful, FPFR-cas demonstrates inferior energy efficiency and economic performance, whereas FPFR-par performs better. PCM24 in FPFR-cas suffers from incomplete solidification. FPFR-cas has the longest *SSP* of 10.39 years. FPFR-par can save up to 2 % more energy and its *SSP* can be reduced by more than 4 years compared to the traditional PCFs employing full heating and thermal storage.

(2) When a local heating method is utilized, changes in the thermal storage method primarily impact the energy savings and economic viability of the PCF heated room. The indoor thermal comfort of rooms with full thermal storage (LPFR-ful) and partial thermal storage (LPFR-par) is essentially the same, while it is slightly diminished in rooms with cascade thermal storage (LPFR-cas). The heating and cooling times are comparable across all three thermal storage methods, with their f_t values differing by no more than 0.1. Furthermore, LPFR-ful and LPFR-par demonstrate better energy savings and economic performance compared to LPFR-cas, with LPFR-par showing superior economic viability. Although LPFR-cas has a slightly higher thermal storage capacity of 3 MJ than the other rooms, the PCM24 within it melts and solidifies poorly. The Q_{Ed} values for LPFR-ful and LPFR-par are essentially equal, at approximately 19.9 kWh/day. Compared to FPFR-ful, both rooms can achieve η values of more than 1.5 %. However, while both have C_d values of approximately 7.8 ¥/day, LPFR-par features a significantly lower *SSP* of 6.49 years.

(3) When the thermal storage method remains constant, variations in the heating method can also affect the heating performance of the PCF room. With full thermal storage, the indoor thermal comfort is enhanced under full heating compared to local heating, although the energy savings and economic viability may be slightly reduced. Compared to LPFR-ful, the T_{tsr} value of FPFR-ful can be increased by more than 1 °C and there is no localized overheating problem, but its η value is slightly lower and the *SSP* is slightly longer. With cascade thermal storage, the local heating method primarily enhances the room's energy savings and economic viability. Compared to FPFR-cas, LPFR-cas shows an increase in the η value of about 10 % and a reduction in the SSP. With partial thermal storage, the indoor thermal comfort in locally heated rooms is improved, while the energy savings and economic viability remain relatively unchanged. Compared to FPFR-par, LPFR-par has a higher f_t value of about 1.45 and its PCM can be fully utilized with an increase in thermal storage capacity of almost 18 MJ.

CRediT authorship contribution statement

Tianyu Wang: Writing – review & editing, Writing – original draft, Visualization, Resources, Methodology, Investigation, Formal analysis, Data curation, Conceptualization. **Haichao Wang:** Writing – review & editing, Supervision, Resources, Project administration, Funding acquisition. **Zhiwen Luo:** Writing – review & editing, Resources, Conceptualization.

Declaration of competing interest

The authors declare that they have no known competing financial interests or personal relationships that could have appeared to influence the work reported in this paper.

Acknowledgements

This work was supported by the China National Key Research and Development Program – China-Finland intergovernmental cooperation in science and technology innovation (2021YFE0116200), academy research fellow funding from Research Council of Finland (Funding No. 334205 and 358055) and NSFC-RS international exchange projects: Digital-twin based smart control of low-carbon heating under climate change (NSFC funding NO. 52311530087 and RS funding NO. 223541).

Data availability

No data was used for the research described in the article.

References

[1] International Energy Agency, Tracking Clean Energy Progress 2023. https://www.iea.org/reports/tracking-clean-energy-progress-2023, 2023 (accessed 9 October 2024).
[2] International Energy Agency, CO_2 Emissions in 2023. https://www.iea.org/reports/co2-emissions-in-2023, 2023 (accessed 9 October 2024).
[3] M.I. Khan, F. Asfand, S.G. Al-Ghamdi, Progress in research and development of phase change materials for thermal energy storage in concentrated solar power, Appl. Therm. Eng. 219 (2023) 119546, https://doi.org/10.1016/j.applthermaleng.2022.119546.
[4] M. Barrio, J. Font, D.O. López, J. Muntasell, J. Ll, Tamarit, Floor radiant system with heat storage by a solid-solid phase transition material, Sol. Energy Mater. Sol. Cells 27 (1992) 127–133, https://doi.org/10.1016/0927-0248(92)90115-6.
[5] X. Sui, H. Liu, Z. Du, S. Yu, Developing a TRNSYS model for radiant cooling floor with a pipe-embedded PCM layer and parametric study on system thermal performance, J. Energy Storage 71 (2023) 108024, https://doi.org/10.1016/j.est.2023.108024.
[6] H. Zhang, Q. Dong, J. Lu, Y. Tang, W. Bi, Y. Gao, H. Yang, J. Wang, Modified sodium acetate trihydrate/expanded perlite composite phase change material encapsulated by epoxy resin for radiant floor heating, J. Energy Storage 65 (2023) 107374, https://doi.org/10.1016/j.est.2023.107374.
[7] B. Sun, Y. Xu, Y. Zhang, H. Zhao, X. Liu, Simulation and optimization research of double energy storage floor based on heat transfer characteristic of phase change materials, J. Energy Storage 51 (2022) 104452, https://doi.org/10.1016/j.est.2022.104452.
[8] X. Jin, X. Zhang, Thermal analysis of a double layer phase change material floor, Appl. Therm. Eng. 31 (2011) 1576–1581, https://doi.org/10.1016/j.applthermaleng.2011.01.023.
[9] Y. Qu, D. Zhou, F. Xue, L. Cui, Multi-factor analysis on thermal comfort and energy saving potential for PCM-integrated buildings in summer, Energ. Buildings 241 (2021) 110966, https://doi.org/10.1016/j.enbuild.2021.110966.
[10] M. Zhao, T. Zhu, C. Wang, H. Chen, Y. Zhang, Numerical simulation on the thermal performance of hydraulic floor heating system with phase change materials, Appl. Therm. Eng. 93 (2016) 900–907, https://doi.org/10.1016/j.applthermaleng.2015.10.020.
[11] Q. Zhang, Z. Yang, G. Wang, Numerical and experimental investigation on dynamic thermal performance of floor heating system with phase change material for thermal storage, Indoor Built. Environ. 30 (2021) 621–634, https://doi.org/10.1177/1420326X19900535.
[12] Y. Zhou, S. Zheng, H. Chen, G. Zhang, Thermal performance and optimized thickness of active shape-stabilized PCM boards for side-wall cooling and under-floor heating system, Indoor Built. Environ. 25 (2016) 1279–1295, https://doi.org/10.1177/1420326X16671983.
[13] X. Xu, Y. Zhang, K. Lin, H. Di, R. Yang, Modeling and simulation on the thermal performance of shape-stabilized phase change material floor used in passive solar buildings, Energ. Buildings 37 (2005) 1084–1091, https://doi.org/10.1016/j.enbuild.2004.12.016.
[14] S. Jeong, J.E. Heo, S. Choi, S. Kim, Heating efficiency enhanced by combination of phase change materials and activated carbon for dry floor heating system, J. Energy Storage 70 (2023) 108027, https://doi.org/10.1016/j.est.2023.108027.
[15] S. Baek, S. Kim, Analysis of thermal performance and energy saving potential by PCM radiant floor heating system based on wet construction method and hot water, Energy 12 (2019) 828, https://doi.org/10.3390/en12050828.
[16] S. Lu, B. Xu, X. Tang, Experimental study on double pipe PCM floor heating system under different operation strategies, Renew. Energy 145 (2020) 1280–1291, https://doi.org/10.1016/j.renene.2019.06.086.
[17] W. Cheng, B. Xie, R. Zhang, Z. Xu, Y. Xia, Effect of thermal conductivities of shape stabilized PCM on under-floor heating system, Appl. Energy 144 (2015) 10–18, https://doi.org/10.1016/j.apenergy.2015.01.055.
[18] B. Larwa, S. Cesari, M. Bottarelli, Study on thermal performance of a PCM enhanced hydronic radiant floor heating system, Energy 225 (2021) 120245, https://doi.org/10.1016/j.energy.2021.120245.

[19] K. Faraj, M. Khaled, J. Faraj, F. Hachem, K. Chahine, C. Castelain, Energetic and economic analyses of integrating enhanced macro-encapsulated PCM's with active underfloor hydronic heating, Energy Rep. 8 (2022) 848–862, https://doi.org/10.1016/j.egyr.2022.07.099.
[20] Q. Yu, B. Sun, C. Li, F. Yan, Y. Li, Analysis of heat charging and release processes in cascade phase change materials energy storage floor heating systems: performance evaluation, J. Energy Storage 78 (2024) 110020, https://doi.org/10.1016/j.est.2023.110020.
[21] Y. Xu, B.B. Sun, L.J. Liu, X.Y. Liu, The numerical simulation of radiant floor cooling and heating system with double phase change energy storage and the thermal performance, J. Energy Storage 40 (2021) 102635, https://doi.org/10.1016/j.est.2021.102635.
[22] S. Cesari, E. Baccega, G. Emmi, M. Bottarelli, Enhancement of a radiant floor with a checkerboard pattern of two PCMs for heating and cooling: results of a real-scale monitoring campaign, Appl. Therm. Eng. 246 (2023) 122887, https://doi.org/10.1016/j.applthermaleng.2024.122887.
[23] S. Lu, J. Gao, H. Tong, S. Yin, X. Tang, X. Jiang, Model establishment and operation optimization of the casing PCM radiant floor heating system, Energy 193 (2020) 116814, https://doi.org/10.1016/j.energy.2019.116814.
[24] Z. Wang, W. Gao, Y. Gao, Influence of hot water pipe position on the performance of radiant floor heating systems integrated with PCM, Case Stud. Therm. Eng. 61 (2024) 105030, https://doi.org/10.1016/j.csite.2024.105030.
[25] Z. Liu, Z. Wei, R. Teng, H. Sun, Z. Qie, Research on performance of radiant floor heating system based on heat storage, Appl. Therm. Eng. 231 (2023) 120812, https://doi.org/10.1016/j.applthermaleng.2023.120812.
[26] S. Baek, S. Kim, Determination of optimum hot-water temperatures for PCM radiant floor-heating systems based on the wet construction method, Sustainability 10 (2018) 4004, https://doi.org/10.3390/su10114004.
[27] R. Barzin, J.J.J. Chen, B.R. Young, M.M. Farid, Application of PCM underfloor heating in combination with PCM wallboards for space heating using price based control system, Appl. Energy 148 (2015) 39–48, https://doi.org/10.1016/j.apenergy.2015.03.027.
[28] S. Cesari, G. Emmi, M. Bottarelli, A weather forecast-based control for the improvement of PCM enhanced radiant floors, Appl. Therm. Eng. 206 (2022) 118119, https://doi.org/10.1016/j.applthermaleng.2022.118119.
[29] X. Kong, L. Jiang, L. Guo, N. Wang, J. Ren, Experimental study on the performance of a stepped phase-change radiation terminal integrated with a building used in summer and winter, J. Energy Storage 62 (2023) 106860, https://doi.org/10.1016/j.est.2023.106860.
[30] T. Wang, H. Wang, Z. Luo, Effects of local heating of phase change floor (PCF) on thermal comfort and energy efficiency, J. Build. Eng. 103 (2025) 112157, https://doi.org/10.1016/j.jobe.2025.112157.
[31] X. Jin, J. Yang, M. Li, G. Huang, A.C.K. Lai, Experimental and numerical study on the thermal energy storage performance of a novel phase-change material for radiant floor heating systems, Build. Environ. 223 (2022) 109491, https://doi.org/10.1016/j.buildenv.2022.109491.
[32] V.R. Voller, C. Prakash, A fixed grid numerical modelling methodology for convection-diffusion mushy region phase-change problems, Int. J. Heat Mass Transf. 30 (1987) 1709–1720, https://doi.org/10.1016/0017-9310(87)90317-6.
[33] W. Chen, Y. Liu, X. Liang, F. Luo, T. Liao, S. Wang, X. Gao, Z. Zhang, Y. Fang, Experimental and numerical investigations on radiant floor heating system integrated with macro-encapsulated phase change material, Energy 282 (2023) 128375, https://doi.org/10.1016/j.energy.2023.128375.
[34] Z. Kang, R. Tan, Q. Yao, J. Zhang, S. Zhang, Y. Wei, Numerical simulation of energy storage radiant floor heating systems with phase change materials having different thermophysical properties, Constr. Build. Mater. 463 (2025) 140010, https://doi.org/10.1016/j.conbuildmat.2025.140010.
[35] Dongguan Chengbang Polymer Material Co. Guangdong, China. https://rl9ym1en.51pla.com/product.htm, 2023 (accessed 9 October 2024).
[36] M.B. Awan, Z. Ma, W. Lin, A.K. Pandey, V.V. Tyagi, A characteristic-oriented strategy for ranking and near-optimal selection of phase change materials for thermal energy storage in building applications, J. Energy Storage 57 (2023) 106301, https://doi.org/10.1016/j.est.2022.106301.
[37] O. Babaharra, K. Choukairy, S. Hamdaoui, K. Khallaki, S.H. Mounir, Thermal behavior evaluation of a radiant floor heating system incorporates a microencapsulated phase change material, Constr. Build. Mater. 330 (2022) 127293, https://doi.org/10.1016/j.conbuildmat.2022.127293.
[38] H. Wang, S. Bo, C. Zhu, P. Hua, Z. Xie, C. Xu, T. Wang, X. Li, H. Wang, R. Lahdelma, K. Granlund, E. Teppo, A zoned group control of indoor temperature based on MPC for a space heating building, Energy Convers. Manag. 290 (2023) 117196, https://doi.org/10.1016/j.enconman.2023.117196.
[39] China Academy of Building Science, Code for Thermal Design of Civil Buildings (GB50176-2016), 2016.
[40] Shandong Weimengshi Technology Co, Temperature and humidity transmitter (Probe 485 type), China. https://www.sdvms.com/index.php?a=shows&catid=76&id=17 (accessed 16 January 2025).
[41] J. Guo, Y. Jiang, A semi-analytical model for evaluating the thermal storage capacity and heat use efficiency of flexible thermal storage heating floor, Appl. Therm. Eng. 198 (2021) 117448, https://doi.org/10.1016/j.applthermaleng.2021.117448.
[42] T. Xu, J. Zhang, G. Fan, T. Zou, H. Hu, Y. Du, Y. Yang, H. Li, P. Huang, Hydrate salt/fumed silica shape-stabilized composite phase change material with adjustable phase change temperature for radiant floor heating system, J. Build. Eng. 71 (2023) 106400, https://doi.org/10.1016/j.jobe.2023.106400.
[43] C.S. (GB), Design Code for Heating Ventilation and Air Conditioning of Civil Buildings (in Chinese), Chinese Standards (GB), 2012.
[44] L. Karim, F. Barbeon, P. Gegout, A. Bontemps, L. Royon, New phase-change material components for thermal management of the light weight envelope of buildings, Energ. Buildings 68 (2014) 703–706, https://doi.org/10.1016/j.enbuild.2013.08.056.
[45] Liaoning Development and Reform Commission, Notice of the provincial development and reform commission on matters relating to further improvement of the time-sharing electricity price mechanism. https://fgw.ln.gov.cn/fgw/index/wndt/20230830180920477788/, 2023 (accessed 9 October 2024).
[46] State Grid Liaoning Electric Power Co., Ltd, Agent to buy electrical commercial users electricity price table. http://www.ln.sgcc.com.cn/html/files/2024-07/15/20240715155138300538836.pdf, 2024 (accessed 9 October 2024).
[47] J. Fernández-Seara, F.J. Uhía, J. Sieres, Experimental analysis of a domestic electric hot water storage tank. Part I: static mode of operation, Appl. Therm. Eng. 27 (2007) 129–136, https://doi.org/10.1016/j.applthermaleng.2006.05.006.
[48] China Academy of Building Science, Technical Specification for Radiant Heating and Cooling (JGJ 142–2012), 2012.